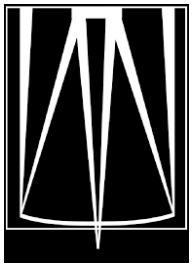

Performance of Various GNAO Observing Modes

GNAO-SYS-SIM-011

Related PBS ID: 5.2

M. van Dam, G. Sivo, E. Marin

November 26, 2020

Table of Contents

Document Acceptance and Release Notice
This document is a managed document. To identify changes, each page contains a release number and a page number. This document is authorized for release once all signatures have been obtained.

APPROVED:	*Approval on file* _____ William Rambold GNAO Project Lead Systems Engineer	Date:	2021-01-14
APPROVED:	*Approval on file* _____ Manuel Lazo GNAO Project Manager	Date:	2021-01-14
APPROVED:	*Approval on file* _____ Gaetano Sivo GNAO Principal Investigator	Date:	2021-01-14
APPROVED:	*Approval on file* _____ Henry Roe GNAO Sponsor, Gemini Deputy Director	Date:	2021-01-14

Change Record

Version	Date	Description	Owner Name	Change Request
1.0	10/5/20	Released through formal change control process	M. van Dam	GEM-180
2.0	10/30/20	Added new GLAO and LTAO results	M. van Dam	GEM-184
3.0	11/13/20	Added 5 LGS and MOAO results	M. van Dam	GEM-230
4.0	11/27/20	Added results from a 3+1 LGS constellation	M. van Dam	GEM-263

1 Introduction

The Gemini North Adaptive Optics (GNAO) instrument is a next generation multi-conjugate adaptive optics (MCAO) system designed for a wide range of science cases. The aim is to produce near diffraction-limited image quality for J-, H- and K-bands. Due to budget constraints, we are interested in comparing the performance of various flavors of AO systems. In this report, we simulate a variety of AO systems and report on their performance.

The performance of the GNAO design is reported in GNAO-SYS-SIM-001,[1] GNAO-SYS-SIM-004[2] and GNAO-SYS-SIM-006.[3]

A similar study of different AO modes is reported in GNAO-SYS-SIM-006.The main difference is that the earlier study applied the different AO modes to the baseline GNAO system. Here, we consider an AO system with a single DM (conjugate to the ground initially and later reconjugated to 9 km) and reconfigurable LGS WFSs that are at the edge of the field (60" off-axis) but can be brought in to 10" off-axis for the LTAO mode.

2 Simulation description

The same files and scripts used to run previous simulations in YAO were used as a starting point. The simulation parameters are the same as GNAO-SYS-SIM-006. In all cases, the LGS WFSs have 20x20 subapertures and all DMs have an interactuator spacing of the same size (0.395 m).

Three different laser launch configurations are used in the simulations. Two lasers are used to create either four or five LGSs. The LGS launch configurations are shown in Figure **1**. The default configuration which is used in the simulations (unless otherwise specified) is the 4 LGS constellation on the left.

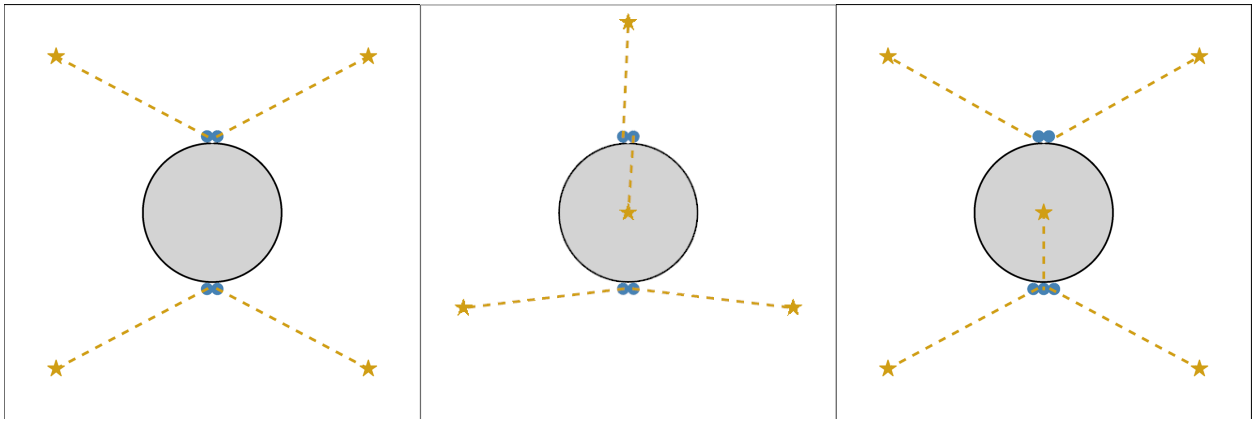

Figure 1: Location of the launch telescopes and guide stars for the 4 LGS constellation (left), the 3+1 LGS constellation (center) and the 5 LGS constellation (right).

[1] Marcos van Dam, Gaetano Sivo and Eduardo Marin, "Simulated Performance of GNAO," GNAO-SYS-SIM-001 v4.0 13 April 2020

[2] Marcos van Dam, Gaetano Sivo and Eduardo Marin, "Wavefront Sensor and Deformable Mirror Design Parameters for GNAO," GNAO-SYS-SIM-004 v3.0 29 April 2020

[3] Marcos van Dam and Gaetano Sivo, "Performance Delivered by All Adaptive Optics Modes in GNAO," GNAO-SYS-SIM-006 ,v1.0, 12 June 2020.

3 Ground Layer Adaptive Optics simulation results

3.1 General simulations

The ground-layer adaptive optics (GLAO) simulations use four LGSs located at the edge of the 2' diameter science field of view to correct the entire field using a deformable mirror (DM) located conjugate to the ground. A single natural guide star (NGS) is used to measure the tip-tilt mode, as well as the slowly varying focus variations due to changes in the sodium altitude.

For the purposes of evaluating the image quality, we generate a grid of stars even distributed over the 2' diameter field, as shown in Figure **2**.

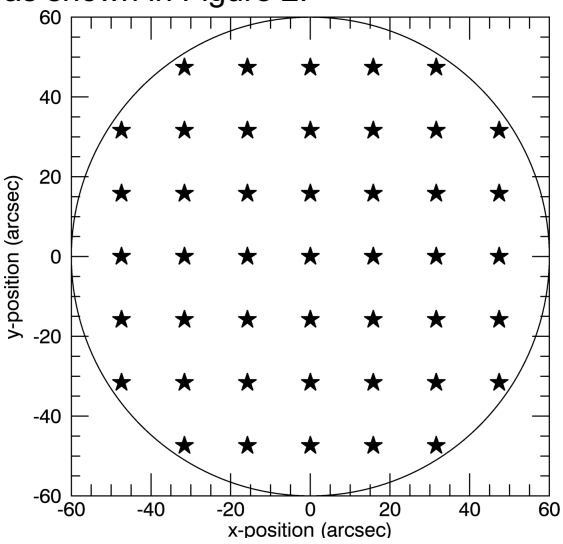

Figure 2: Location of the science targets used to optimize the wavefront correction and to evaluate the image quality delivered by GLAO system.

The Rayleigh contamination depends on the Cass Rotator Angle, which rotates the location of the laser guide star launch teescopes relative to the pupil. All the work until now has used the best Cass Rotator Angle, which we denote as 0º in Figure **3**. However, as the telescope tracks a star, the Cass Rotator will rotate and the Rayleigh backscatter will increase. Nevertheless, the relative number of contanimated subapertures is small and the performance is not affected provided that the reconstructor knows which subapertures to ignore.

Figure 3: Rayleigh pattern in GLAO mode for a pupil rotation of, from left to right, 0º, 30º and 60º. For each position, four LGS WFSs corresponding to LGSs 60" from the optical axis are shown.

The Strehl ratio at J-, H- and K-band as a function of tip-tilt guide star location is tabulated

in Table **1**, and the contour plot of the K-band values shown in Figure **4**.

Tip-tilt GS	[0”,0”]	[30”,0”]	[60”,0”]
J-band	0.064 ± 0.016	0.062 ± 0.015	0.056 ± 0.010
H-band	0.166 ± 0.042	0.162 ± 0.040	0.143 ± 0.030
K-band	0.334 ± 0.062	0.324 ± 0.067	0.295 ± 0.058

Table 1: Simulated mean and standard deviation in J-, H-, K-band Strehl ratio as a function of the location of the tip-tilt guide star using the median turbulence profile for an observation at zenith.

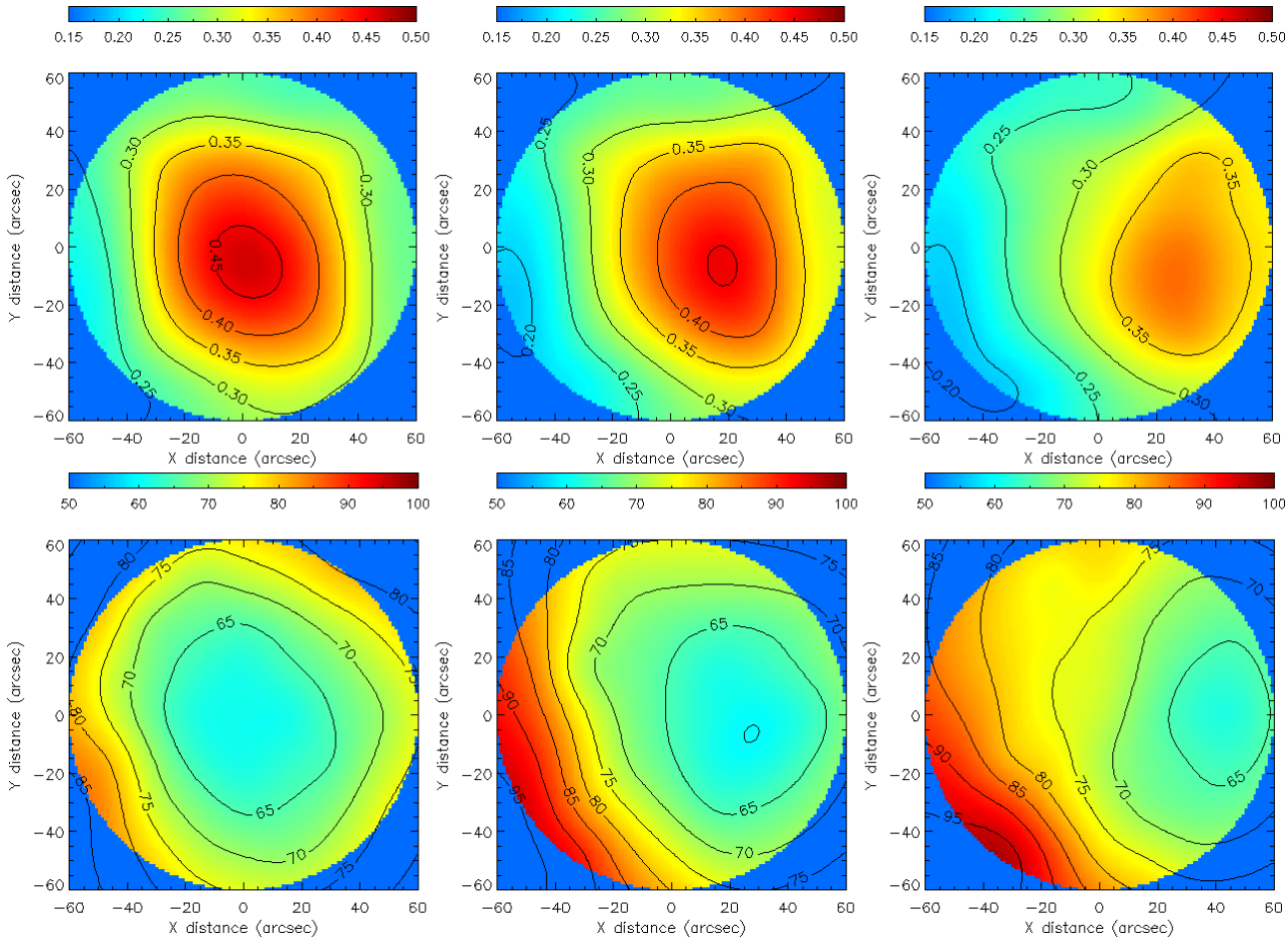

Figure 4: K-band Strehl ratio (top) and FWHM (bottom) for a tip-tilt star at, from left to right, [0”, 0”], [30”, 0”] and [60”, 0”].

The simulations that follow all have the tip-tilt guide star at the center of the field. The Strehl ratio and FWHM as a function of zenith angle are tabulated in Tables **2** and **3** respectively.

Zenith angle	0º	25º	50º
J-band	0.064 ± 0.016	0.046 ± 0.011	0.019 ± 0.003
H-band	0.166 ± 0.042	0.124 ± 0.030	0.050 ± 0.013
K-band	0.334 ± 0.062	0.271 ± 0.052	0.126 ± 0.036

Table 2: Simulated mean and standard deviation in J-, H-, K-band Strehl ratio as a function of zenith angle for the median turbulence profile.

Zenith angle	0º	25º	50º
J-band	73.4 ± 19.8	92.8 ± 23.1	164.1 ± 26.3
H-band	63.0 ± 9.6	71.8 ± 12.6	124.4 ± 30.6
K-band	69.6 ± 5.6	74.4 ± 6.9	106.9 ± 23.0

Table 3: Simulated mean and standard deviation in J-, H-, K-band FWHM (mas) as a function of zenith angle for the median turbulence profile.

Table **4** shows the Strehl ratio at zenith for three different seeing conditions.

Percentile	25	50	75
J-band	0.131 ± 0.031	0.064 ± 0.016	0.024 ± 0.005
H-band	0.277 ± 0.055	0.166 ± 0.042	0.077 ± 0.023
K-band	0.466 ± 0.062	0.334 ± 0.062	0.198 ± 0.051

Table 4: Simulated mean and standard deviation in J-, H-, K-band Strehl ratio as a function of seeing percentile.

3.2 Simulations using a 3+1 LGS constellation

A subset of the GLAO simulations in Section 3.1 were repeated using three LGSs in an equilateral triangle at a radial distance of 50" plus a central LGS. The results in Tables **6** and **8** show that average performance is better for the 3+1 LGS constellation, but the variation is also higher.

Zenith angle	0°	25°	50°
J-band	0.071 ± 0.025	0.049 ± 0.016	0.020 ± 0.006
H-band	0.178 ± 0.054	0.113 ± 0.041	0.054 ± 0.021
K-band	0.348 ± 0.077	0.283 ± 0.066	0.135 ± 0.050

Table 5: Simulated mean and standard deviation in J-, H-, K-band Strehl ratio as a function of zenith angle for a 3+1 LGS GLAO system.

Percentile	25	50	75
J-band	0.142 ± 0.041	0.071 ± 0.025	0.028 ± 0.010
H-band	0.291 ± 0.067	0.178 ± 0.054	0.086 ± 0.033
K-band	0.478 ± 0.074	0.348 ± 0.077	0.212 ± 0.066

Table 6: Simulated mean and standard deviation in J-, H-, K-band Strehl ratio as a function of seeing percentile for a 3+1 LGS GLAO system.

The contour plots for the Strehl ratio and FWHM at zenith under median seeing conditions is shown in Figure **5**.

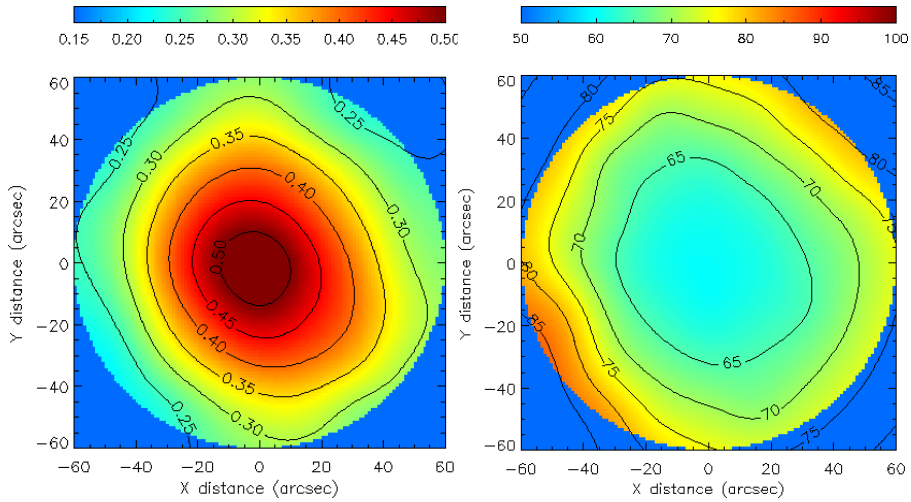

Figure 5: K-band Strehl ratio (teft) and FWHM (right) for a tip-tilt star at [0", 0"], [30", 0"] using the 3+1 LGS constellation.

3.3 Simulations using a 5 LGS constellation

A subset of the GLAO simulations in Section 3.1 were repeated using the 5 LGS constellation, including a central LGS and four LGSs situated 60" off-axis. Table **7** shows that adding a star at the center of the field increases the Strehl ratio of a GLAO system by a small amount. The reason for this is that the performance is limited by the fact that there is a single DM, not the inability to sense the performance on-axis. The remainder of the simulations in this section use four LGSs.

Percentile	25	50	75
J-band	0.142 ± 0.044	0.071 ± 0.027	0.028 ± 0.011
H-band	0.291 ± 0.078	0.178 ± 0.058	0.087 ± 0.036
K-band	0.478 ± 0.075	0.348 ± 0.079	0.213± 0.069

Table 7: Simulated mean and standard deviation in J-, H-, K-band Strehl ratio as a function of seeing percentile for a 5 LGS GLAO system.

3.4 Subaperture size optimization

Simulations were run to understand what effect of the subaperture size and actuator density have on GLAO performance. The number of subapertures across the pupil was varied between 12x12 to 32x32, with one more actuator than subaperture across the pupil (i.e.,13x13 to 33x33 actuators). The results are tabulated in Table **8**.

Subap	12x12	16x16	20x20	24x24	28x28	32x32
J-band	0.057±0.014	0.061±0.016	0.064±0.016	0.064±0.017	0.065±0.017	0.064±0.017
H-band	0.155±0.039	0.162±0.041	0.166±0.041	0.166±0.042	0.167±0.042	0.166±0.042
K-band	0.322±0.060	0.331±0.062	0.335±0.062	0.334±0.062	0.336±0.063	0.335±0.063

Table 8: Simulated mean and standard deviation in J-, H-, K-band Strehl ratio as a function of number of subapertures using the median turbulence profile for an observation at zenith.

The performance depends only weakly on the number of subapertures, and using more than 20x20 does not provide any additional benefit in median seeing.

4 Laser Tomography Adaptive Optics simulation results

4.1 General simulations

The laser tomography adaptive optics (LTAO) simulations use four LGSs located at a distance of 10” from the optical axis to provide AO correction over an 8”x8” field. The image quality was evaluated using a 5x5 grid of stars evenly distributed in an 8”x8” square region. The Rayleigh backscatter for this LGS constellation is shown in Figure **6** for three different angles.

Figure 6: Rayleigh pattern in LTAO mode for a pupil rotation of, from left to right, 0º, 30º and 60º. For each position, four LGS WFSs corresponding to LGSs 10” from the optical axis are shown.

The Strehl ratio at J-, H- and K-band as a function of tip-tilt guide star location, zenith angle and turbulence profile are tabulated in Tables **9**, **10** and **11**.

Tip-tilt GS	[0”,0”]	[30”,0”]	[60”,0”]
J-band	0.632 ± 0.038	0.491 ± 0.025	0.267 ± 0.015
H-band	0.768 ± 0.027	0.654 ± 0.020	0.419 ± 0.017
K-band	0.861 ± 0.017	0.783 ± 0.014	0.583 ± 0.012

Table 9: Simulated mean and standard deviation in J-, H-, K-band Strehl ratio as a function of the location of the tip-tilt guide star using the median turbulence profile for an observation at zenith.

Zenith angle	0º	25º	50º
J-band	0.632 ± 0.038	0.595 ± 0.048	0.409 ± 0.063
H-band	0.768 ± 0.027	0.741 ± 0.035	0.595 ± 0.054
K-band	0.861 ± 0.017	0.844 ± 0.022	0.745 ± 0.038

Table 10: Simulated mean and standard deviation in J-, H-, K-band Strehl ratio as a function of zenith angle for the median turbulence profile.

Percentile	25	50	75
J-band	0.719 ± 0.031	0.632 ± 0.038	0.504 ± 0.045
H-band	0.827 ± 0.021	0.768 ± 0.027	0.673 ± 0.035
K-band	0.898 ± 0.013	0.861 ± 0.017	0.799 ± 0.024

Table 11: Simulated mean and standard deviation in J-, H-, K-band Strehl ratio as a

function of seeing percentile.

The K-band Strehl ratio across the field is plotted in Figure **7**.

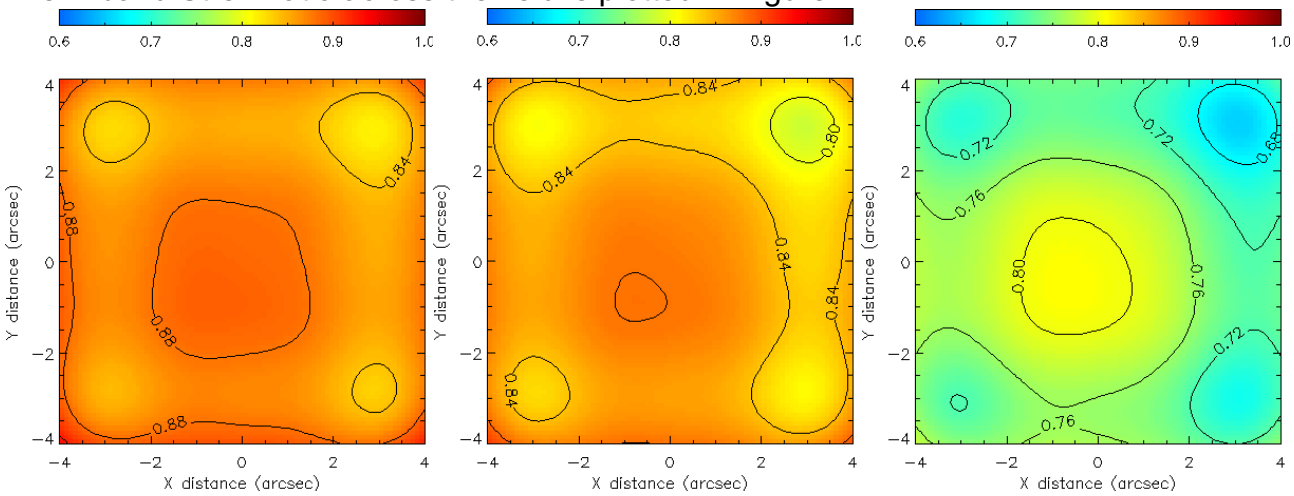

Figure 7: K-band Strehl ratio over an 8”x8” field of view for the LTAO mode for zenith angles of, from left to right, 0º, 25º and 50º.

4.2 Subaperture size optimization

The number of subapertures across the pupil was varied between 16x16 to 32x32. The number of actuators was one more than the number of subapertures (i.e.,13x13 to 33x33). The on-axis Strehl ratio is relatively insensitive to the number of subapertures, and using more than 20x20 does not provide any additional benefit in median seeing (Table **12**).

Subap	16x16	20x20	24x24	28x28	32x32
K-band	0.872	0.882	0.885	0.888	0.898

Table 12: Simulated on-axis K-band Strehl ratio as a function of number of subapertures using the median turbulence profile for an observation at zenith.

4.3 Laser guide star location

In LTAO mode, the main function of using multiple guide stars is to eliminate the cone effect by sampling the whole cylinder of turbulence above the telescope. In order to achieve this, the off-axis guide stars must be 9” from the optical axis for observations at zenith. The on-axis performance as a function of off-axis distance of the guide stars is tabulated in Table **13**.

	6”	8”	10”	12”	14”	16”	18”	20”	22”	24”
0º	0.875	0.882	0.887	0.881	0.871	0.863	0.854	0.842	0.827	0.812
25º	0.879	0.886	0.880	0.871	0.858	0.845	0.831	0.813	0.796	0.779
50º	0.834	0.820	0.811	0.788	0.755	0.727	0.690	0.670	0.637	0.596

Table 13: Simulated on-axis K-band Strehl ratio as a function of guide star off-axis distance using the median turbulence profile for zenith angles of 0º, 25º and 50º.

The K-band results are plotted in Figure **8**. Note that for observations away from zenith, the optimal guide star position is closer to the optical axis.

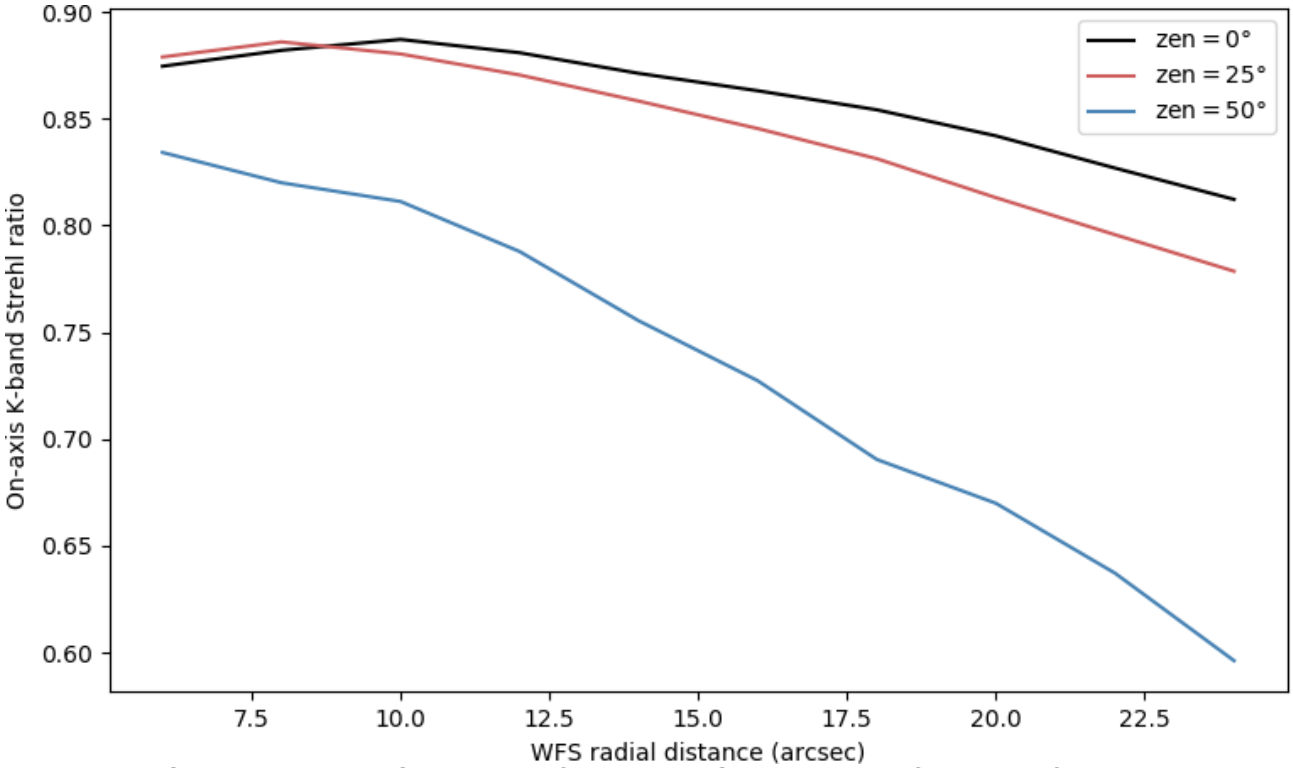

Figure 8: On-axis K-band Strehl ratio for the LTAO mode as a function of radial distance of the four LGS WFSs. The zenith angles are 0º, 25º and 50º.

4.4 Wide field LTAO

In this section, we show how an LTAO system could be used to produce excellent and uniform correction over a wider field of view. Here, we consider a corrected 20”x20” field of view using 4 LGS WFSs situatied at the corners of the field of view. In the first case, we use the regular LTAO reconstructor which optimizes on-axis, while in the second case, we create a reconstructor that minimizes the wavefront error over the 20”x20” field. The results are summarized in Table **14**. With the wide-field reconstructor we attain more uniform performance across the field of view, at the cost of reducing the on-axis performance, as shown in Figure **9**.

Reconstructor	On-axis			Wide-field		
	Min	Mean	Max	Min	Mean	Max
J-band	0.212	0.407	0.646	0.266	0.439	0.613
H-band	0.408	0.590	0.777	0.465	0.618	0.755
K-band	0.603	0.740	0.868	0.648	0.761	0.853

Table 14: Simulated mean and standard deviation in J-, H-, K-band Strehl ratio as a function of seeing percentile.

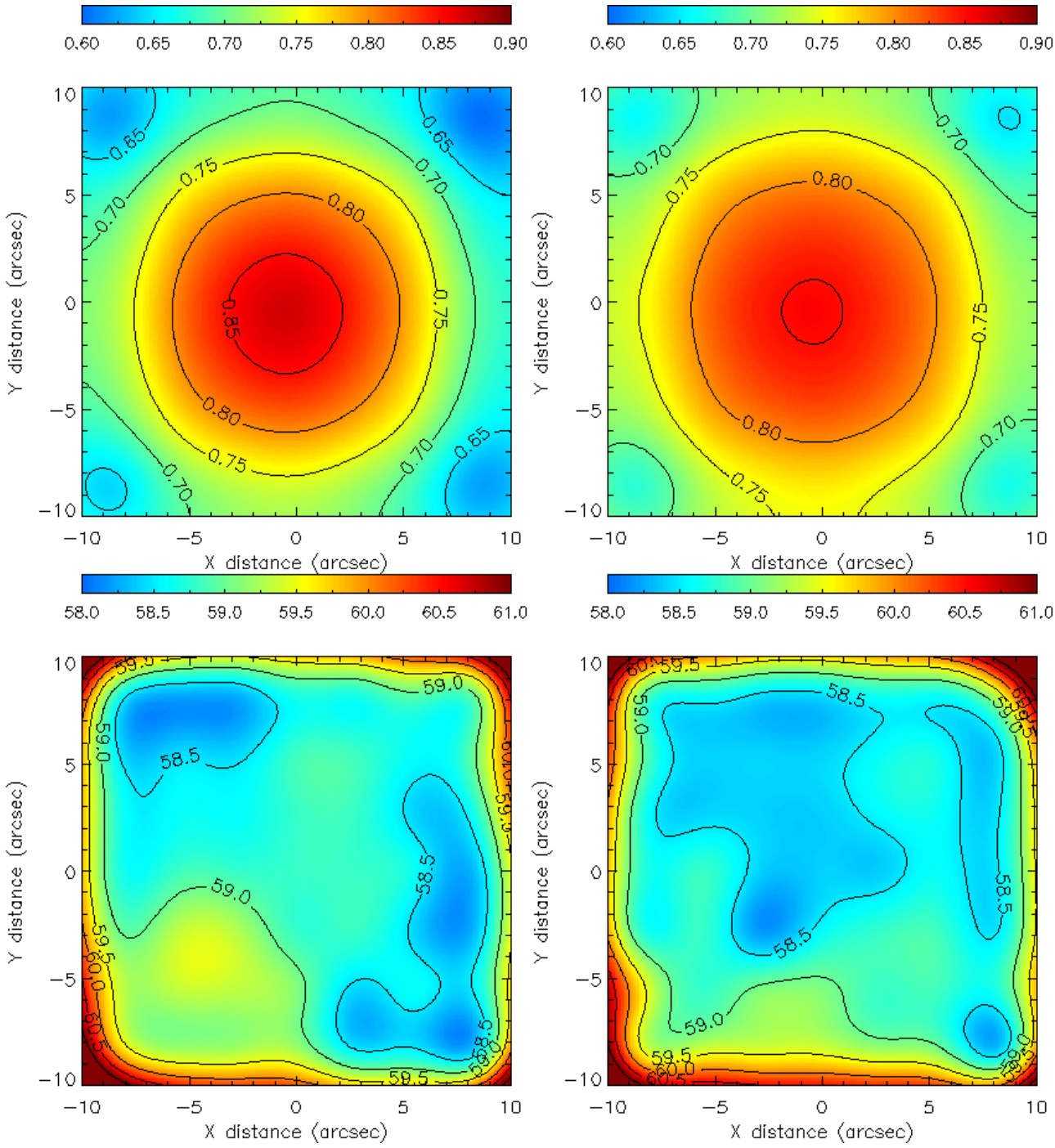

Figure 9: K-band Strehl ratio (top) and FWHM (bottom) for the LTAO mode over a 20”x20” field using two reconstruction strategies: optimizing on-axis (left), and optimizing over the entire field (right).

The question arises as to how the performance of the LTAO system changes with field of view if the LGS constellation is made wider and the performance is optimized over the entire field of view. Simulations were run with increasingly wider science fields of view with the four LGSs at the corner of the science field. The results show in Figure **10** show that the mean performance over a 40”x40” field using an LTAO system with an on-axis NGS is comparable to that of an MCAO system with 5 LGSs and 3 NGSs over an 85”x85” field of view (see Section 5.2).

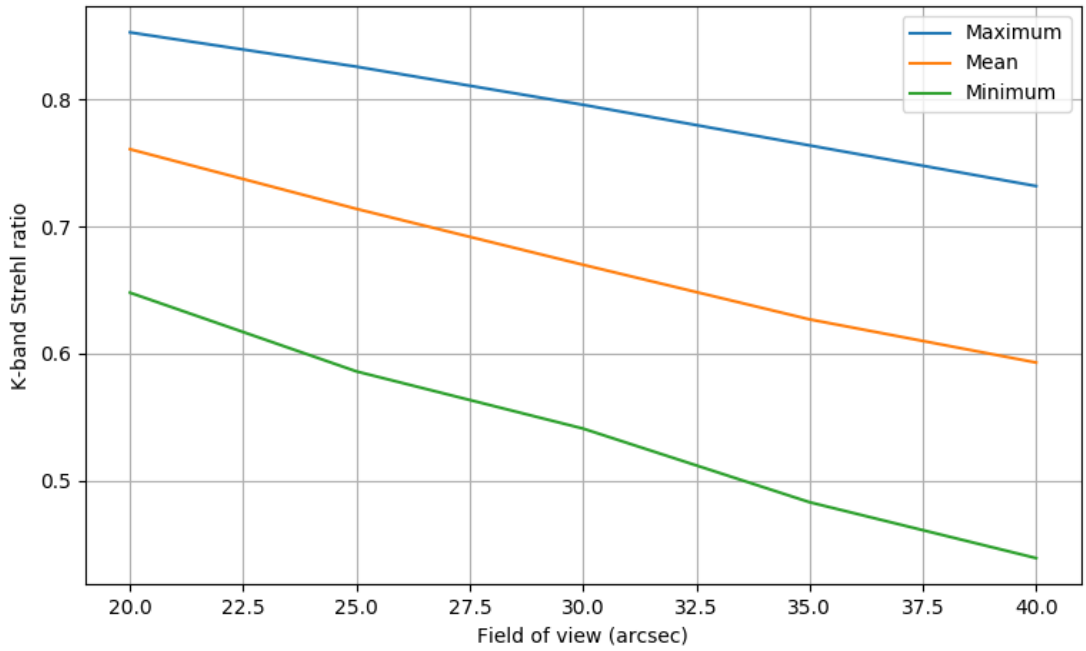

Figure 10: On-axis K-band Strehl ratio for the LTAO mode as a function of radial distance of the four LGS WFSs. The zenith angles are 0º, 25º and 50º.

4.5 Wide-field LTAO using a 3+1 LGS constellation

The wide-field LTAO simulations in were repeated using three LGSs in an equilateral triangle at a radial distance of 50" plus a central LGS. The guide stars are at a much larger off-axis distance than the science targets (20"x20") because the radius of the asterism cannot be adjusted when there is a central guide star. The results in Tables **15** and **16** demonstrate that there is a reduction in Strehl ratio in LTAO if the angle of the guide stars cannot be reduced. The mean K-band Strehl is reduced from 0.761 to 0.723.

Zenith angle	0°	25°	50°
J-band	0.377 ± 0.076	0.325 ± 0.083	0.137 ± 0.075
H-band	0.565 ± 0.066	0.516 ± 0.079	0.296 ± 0.101
K-band	0.723 ± 0.048	0.685 ± 0.060	0.490 ± 0.099

Table 15: Simulated mean and standard deviation in J-, H-, K-band Strehl ratio as a function of zenith angle for a 3+1 LGS LTAO system optimized over a 20"x20" region.

Percentile	25	50	75
J-band	0.487 ± 0.068	0.377 ± 0.076	0.248 ± 0.072
H-band	0.658 ± 0.054	0.565 ± 0.066	0.439 ± 0.076
K-band	0.789 ± 0.037	0.723 ± 0.048	0.625 ± 0.063

Table 16: Simulated mean and standard deviation in J-, H-, K-band Strehl ratio as a function of seeing percentile for a 3+1 LGS LTAO system optimized over a 20"x20" region.

4.6 Wide-field LGS AO using a single LGS

The question arose about the performance of LGS AO feasibility of using a single on-axis

LGS with all of the power from a single laser. The simulation results in Tables **17** and **18** indicate that ...

Zenith angle	0°	25°	50°
J-band	0.354 ± 0.075	0.294 ± 0.082	0.137 ± 0.080
H-band	0.542 ± 0.070	0.482 ± 0.082	0.289 ± 0.108
K-band	0.704 ± 0.053	0.658 ± 0.065	0.479 ± 0.106

Table 17: Simulated mean and standard deviation in J-, H-, K-band Strehl ratio as a function of zenith angle for an on-axis LGS system evaluated over a 20”x20” region.

Percentile	25	50	75
J-band	0.468 ± 0.072	0.354 ± 0.075	0.225 ± 0.067
H-band	0.640 ± 0.059	0.542 ± 0.070	0.410 ± 0.076
K-band	0.776 ± 0.041	0.704 ± 0.053	0.598 ± 0.066

Table 18: Simulated mean and standard deviation in J-, H-, K-band Strehl ratio as a function of seeing percentile for am on-axis LGS system evaluated over a 20”x20” region.

5 Multiconjugate Adaptive Optics simulation results

5.1 MCAO with 4 LGS, 3 NGS

The MCAO simulations consist of an adaptive secondary mirror (ASM) conjugate to -97 m, and the DM used in the previous simulations now reconjugated to the higher altitude of 9 km (based on the results of GNAO-SYS-SIM-001).[4] In this section, we consider the same 4 LGS constellation described by Figure 1, with three NGSs used to measure tip-tilt and the plate scale modes. The location of the three NGSs is [0, +35], [+40 , -30] and [-40 , -20].

The Strehl ratio at J-, H- and K-band as a function of zenith angle and turbulence profile are tabulated in Tables **19** and **20**.

Zenith angle	0º	25º	50º
J-band	0.179±0.023	0.141±0.021	0.044±0.010
H-band	0.360±0.029	0.312±0.029	0.134±0.022
K-band	0.557±0.028	0.513±0.029	0.298±0.031

Table 19: Simulated mean and standard deviation in J-, H-, K-band Strehl ratio as a function of zenith angle for the median turbulence profile.

Percentile	25	50	75
J-band	0.291±0.031	0.179±0.023	0.080±0.013
H-band	0.483±0.033	0.360±0.029	0.220±0.022
K-band	0.660±0.027	0.557±0.028	0.418±0.026

Table 20: Simulated mean and standard deviation in J-, H-, K-band Strehl ratio as a

[4] “Simulated Performance of GNAO,” Marcos van Dam, Gaetano Sivo and Eduardo Marin, GNAO-SYS-SIM-001 v3.3 13 April 2020

function of seeing percentile.

5.2 MCAO with 5 LGS, 3 NGS

The simulations were repeated with an additional LGS at the center, using the launch configuration. The Strehl ratio at J-, H- and K-band as a function of zenith angle and turbulence profile are tabulated in Tables **21** and **22**.

Zenith angle	0º	25º	50º
J-band	0.238±0.040	0.193±0.039	0.054±0.014
H-band	0.429±0.046	0.377±0.049	0.157±0.030
K-band	0.616±0.041	0.571±0.046	0.332±0.040

Table 21: Simulated mean and standard deviation in J-, H-, K-band Strehl ratio as a function of zenith angle for the median turbulence profile.

Percentile	25	50	75
J-band	0.355±0.043	0.238±0.040	0.123±0.030
H-band	0.545±0.042	0.429±0.046	0.287±0.045
K-band	0.707±0.034	0.616±0.041	0.488±0.047

Table 22: Simulated mean and standard deviation in J-, H-, K-band Strehl ratio as a function of seeing percentile.

5.3 MCAO with 4 LGS, 1 NGS

The simulations were repeated using only a single NGS. In this case, it is not possible to correct for the tip-tilt anisoplanatism since there is only one tip-tilt measurement. Initially, the long exposure Strehl ratio was very bad, because the reconstructor allows quadratic modes in the high-altitude DM. The reconstructor was tweaked to remove focus and astigmatism from the high-altitude DM and this resulted in vastly improved performance. However, this should really happen in the tomographic reconstruction stage, and needs some work; it is possible that the Strehl ratio could be further improved.

The Strehl ratio at J-, H- and K-band as a function of tip-tilt guide star location, zenith angle and turbulence profile are tabulated in Tables **23**, **24** and **25**.

Tip-tilt GS	[0”,0”]	[30”,0”]	[60”,0”]
J-band	0.130±0.018	0.113±0.027	0.092±0.022
H-band	0.284±0.035	0.252±0.050	0.203±0.043
K-band	0.478±0.040	0.438±0.061	0.365±0.064

Table 23: Simulated mean and standard deviation in J-, H-, K-band Strehl ratio as a function of the location of the tip-tilt guide star using the median turbulence profile for an observation at zenith.

Zenith angle	0º	25º	50º
J-band	0.130±0.018	0.107±0.017	0.037±0.006
H-band	0.284±0.035	0.252±0.034	0.114±0.022

K-band	0.478±0.040	0.445±0.042	0.263±0.041

Table 24: Simulated mean and standard deviation in J-, H-, K-band Strehl ratio as a function of zenith angle for the median turbulence profile.

Percentile	25	50	75
J-band	0.223±0.029	0.130±0.018	0.056±0.008
H-band	0.403±0.039	0.284±0.035	0.161±0.023
K-band	0.590±0.037	0.478±0.040	0.336±0.038

Table 25: Simulated mean and standard deviation in J-, H-, K-band Strehl ratio as a function of seeing percentile.

5.4 MCAO with 5 LGS, 1 NGS

The Strehl ratio at J-, H- and K-band as a function of tip-tilt guide star location, zenith angle and turbulence profile are tabulated in Tables **26**, **27** and **28**. These results may benefit from an improved reconstruction strategy that prevents quadratic modes on the high-altitude DMs.

Tip-tilt GS	[0”,0”]	[30”,0”]	[60”,0”]
J-band	0.192±0.070	0.157±0.047	0.111±0.026
H-band	0.362±0.089	0.314±0.071	0.236±0.050
K-band	0.550±0.083	0.499±0.077	0.405±0.070

Table 26: Simulated mean and standard deviation in J-, H-, K-band Strehl ratio as a function of the location of the tip-tilt guide star using the median turbulence profile for an observation at zenith.

Zenith angle	0º	25º	50º
J-band	0.192±0.070	0.159±0.059	0.054±0.032
H-band	0.362±0.089	0.323±0.079	0.146±0.064
K-band	0.550±0.083	0.514±0.078	0.304±0.087

Table 27: Simulated mean and standard deviation in J-, H-, K-band Strehl ratio as a function of zenith angle for the median turbulence profile.

Percentile	25	50	75
J-band	0.296±0.082	0.192±0.070	0.098±0-.047
H-band	0.477±0.087	0.362±0.089	0.232±0.078
K-band	0.650±0.073	0.550±0.083	0.418±0.090

Table 28: Simulated mean and standard deviation in J-, H-, K-band Strehl ratio as a function of seeing percentile.

6 Multiobject Adaptive Optics simulation results

In this section, we calculate the potential performance of a multiobject adaptive optics (MOAO) system in the following manner. A simulation is run with a single DM, but rather than optimizing the performance over the whole field, we simply optimize and evaluate at

the performance of the AO system in a single direction. The simulation is repeated over the whole field. At a later date, a simulation of a GLAO system followed by GIRMOS-like MOAO correction in the direction of the science targets will be implemented. The aim of these simulations is to compare the expected performance of a GLAO + MOAO system using four or five LGSs.

6.1 MOAO with 4 LGS, 1 NGS

The simulations were first run with 4 LGS and a single on-axis NGS. The Strehl ratio as a function of zenith angle and passband is tabulated in **Table 29** and plotted in **Figure 11**.

Zenith angle	0º	25º	50º
J-band	0.157 ± 0.028	0.115 ± 0.023	0.033 ± 0.009
H-band	0.316 ± 0.039	0.254 ± 0.037	0.091 ± 0.022
K-band	0.502 ± 0.041	0.438 ± 0.047	0.213 ± 0.041

Table 29: Simulated mean and standard deviation in J-, H-, K-band Strehl ratio as a function of zenith angle for the median turbulence profile.

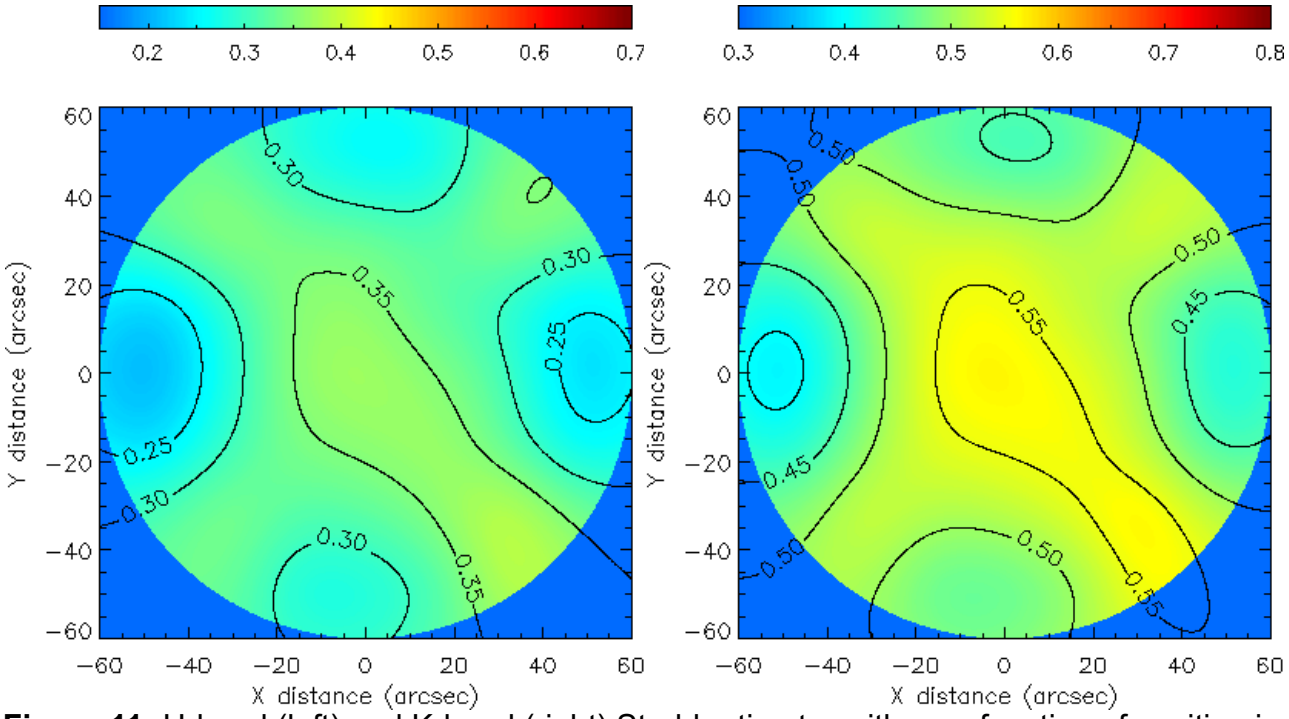

Figure 11: H-band (left) and K-band (right) Strehl ratio at zenith as a function of position in the field using MOAO with 4 LGS. There is one tip-tilt star at the center of the field.

6.2 MOAO with 3+1 LGS, 1 NGS

The simulations were repeated using the 3+1 LGS constellation, where there are three LGSs at a radius of 50" and one LGS on-axis. There is also a single on-axis NGS. **Table 30** displays the Strehl ratio as a function of zenith angle and passband. The contour plots, **Figure 12**, show excellent image quality can be attained at the center and in the direction of the LGSs.

Zenith angle	0º	25º	50º
J-band	0.218 ± 0.092	0.179 ± 0.088	0.056 ± 0.054

H-band	0.381 ± 0.108	0.333 ± 0.111	0.135 ± 0.085
K-band	0.556 ± 0.102	0.512 ± 0.110	0.273 ± 0.109

Table 30: Simulated mean and standard deviation in J-, H-, K-band Strehl ratio as a function of zenith angle for the median turbulence profile for MOAO with the 3+1 asterism.

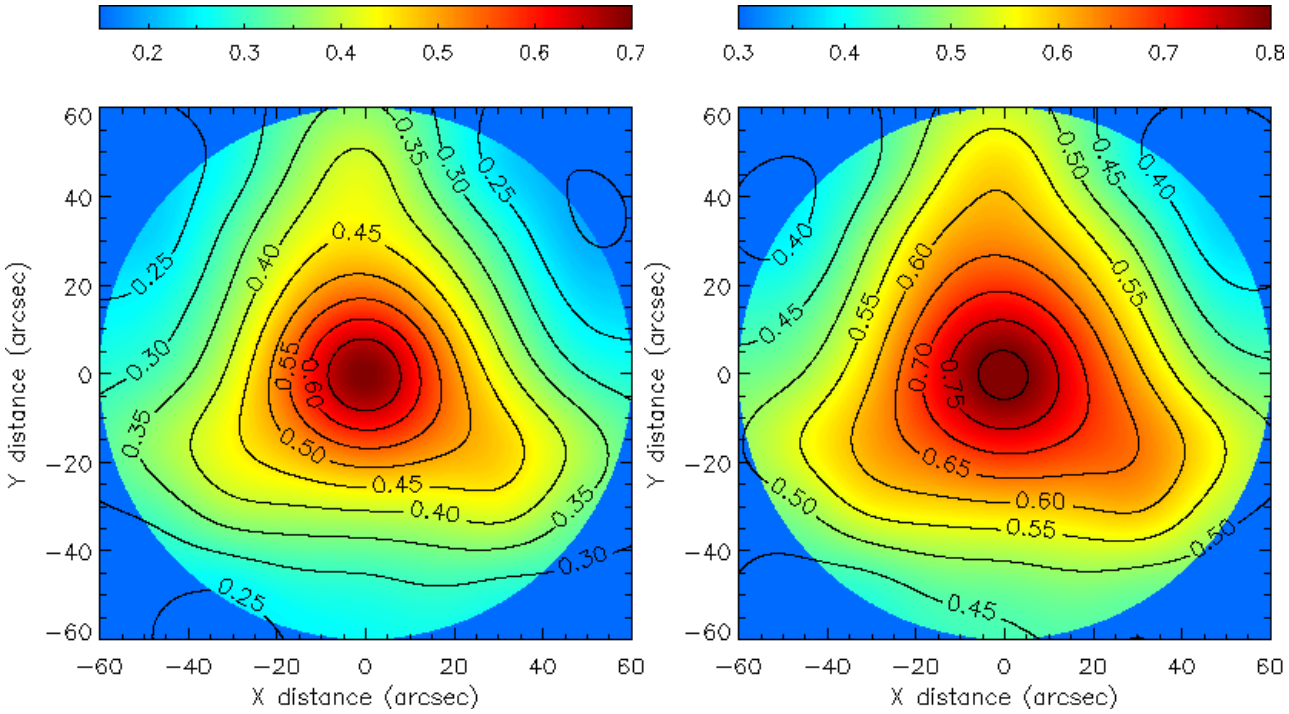

Figure 12: H-band (left) and K-band (right) Strehl ratio at zenith as a function of position in the field using MOAO with 3+1 LGS. There is one tip-tilt star at the center of the field.

6.3 MOAO with 5 LGS, 1 NGS

A third set of simulations was run with 5 LGSs, with the results tabulated in **Table 31**.

Zenith angle	0º	25º	50º
J-band	0.211 ± 0.074	0.165 ± 0.072	0.051 ± 0.045
H-band	0.375 ± 0.087	0.316 ± 0.090	0.125 ± 0.073
K-band	0.555 ± 0.080	0.496 ± 0.088	0.260 ± 0.095

Table 31: Simulated mean and standard deviation in J-, H-, K-band Strehl ratio as a function of zenith angle for the median turbulence profile using the 5 LGS asterism and one tip-tilt star at the center..

The contour plots in **Figure 13** show that the Strehl ratio is much higher near the center of the field compared with the four LGS case, and amost exactly the same elsewhere.

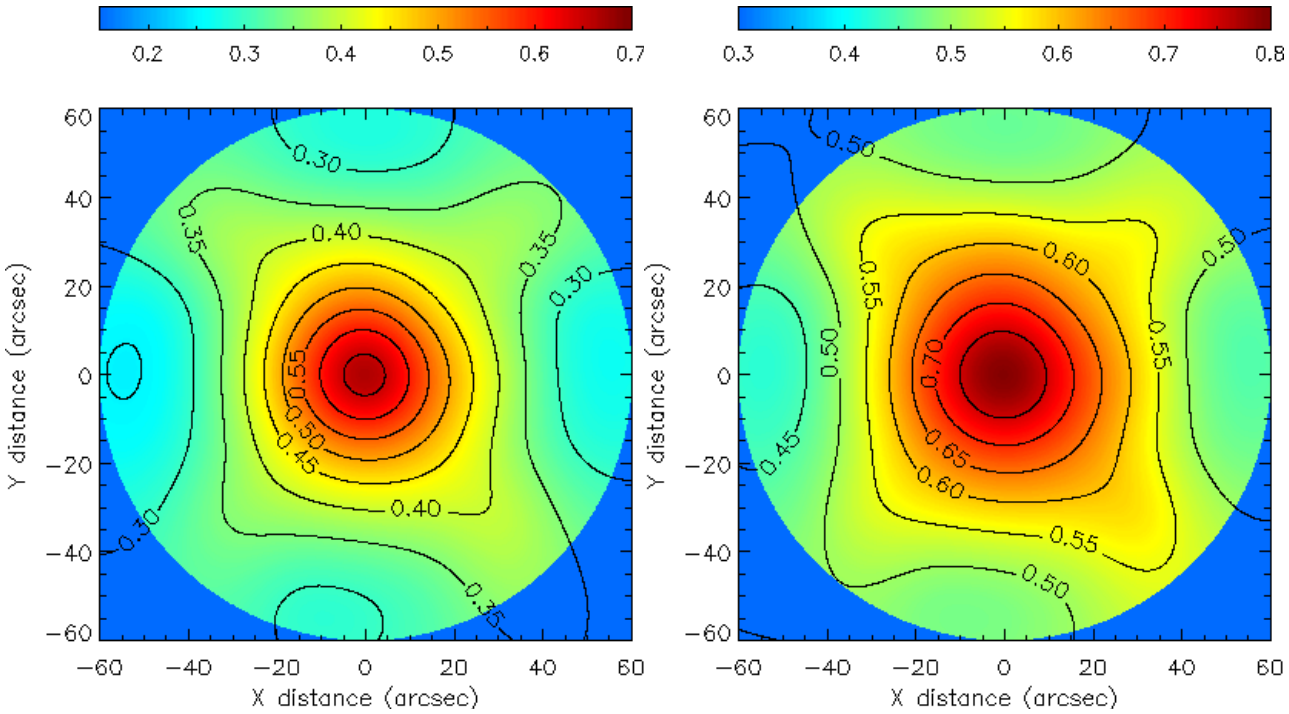

Figure 13: H-band (left) and K-band (right) Strehl ratio at zenith as a function of position in the field using MOAO with 5 LGS. There is one tip-tilt star at the center of the field.

7 Discussion

In this report, we show the results of simulations of an AO system with a simpler optical design than GNAO.

Using a single DM conjugate to the ground, a GLAO system can deliver a K-band Strehl ratio of 0.334 over a 2' diameter field of view. The same system could be used for narrowfield imaging in LTAO mode, with a corresponding Strehl ratio of 0.861. Both of these modes could be scientifically very useful. An additional mode to consider is the wide field LTAO mode where the LGS WFSs are placed further from the optical axis and the correction is optimized over a large field of view. This produces excellent image over a field of view as large as 40"x40".

If an ASM is added to the telescope, the DM could be reconjugated and the system converted to an MCAO system. In this case, the Strehl ratios are slightly lower than what was predicted for GNAO, but still produce diffraction-limited images over the full field of view, even at J-band.